

# Altered modular organization of intrinsic brain functional networks in patients with Parkinson's disease

Qing Ma<sup>1</sup> · Biao Huang<sup>2</sup> · Jinhui Wang<sup>3,4</sup> · Carol Seger<sup>1,5</sup> ·  
Wanqun Yang<sup>2</sup> · Changhong Li<sup>1</sup> · Junjing Wang<sup>1</sup> · Jieying Feng<sup>2</sup> ·  
Ling Weng<sup>1</sup> · Wenjie Jiang<sup>1</sup> · Ruiwang Huang<sup>1</sup>

© Springer Science+Business Media New York 2016

**Abstract** Although previous studies reported altered topology of brain functional networks in patients with Parkinson's disease (PD), the modular organization of brain functional networks in PD patients remains largely unknown. Using the resting-state functional MRI (R-fMRI) and graph theory, we examined the modular organization of brain functional networks in 32 unmedicated patients with early-to-mid motor stage PD and 31 healthy controls. Compared to the controls, the PD patients tended to show decreased integrity and segregation, both within and between modules. This was inferred by significantly increased intra-modular characteristic path length ( $L_p$ ) within four modules: mPFC, SN, SMN, and FPN, decreased inter-modular functional connectivity (FC)

between mPFC and SN, SMN, and VN, and decreased intra-modular clustering in the PD patients. Intra-modular characteristic path length within the mPFC showed significantly positive correlation with general cognitive ability in the PD group. Receiver operating characteristic (ROC) analysis revealed that FC between mPFC and SN had the highest significant accuracy in differentiating the patients from the controls. Our findings may provide new insight in understanding the pathological changes that underlie impairment in cognition and movement in Parkinson's disease.

**Keywords** Modularity · Graph theory · Medial prefrontal cortex (mPFC) · Salience network (SN)

## Highlights

- Characterized altered modular organization in PD patients at early-to-mid clinical motor stages.
- PD patients showed increased intra-modular path length in mPFC, SN, FPN, and SMN.
- Characteristic path length changed when confronted with 'module lesion'
- Inter-modular functional connectivity between mPFC and SN can differentiate PD patients from controls.

Qing Ma and Biao Huang contributed equally to this work.

**Electronic supplementary material** The online version of this article (doi:10.1007/s11682-016-9524-7) contains supplementary material, which is available to authorized users.

✉ Biao Huang  
cjr.huangbiao@vip.163.com

✉ Ruiwang Huang  
ruiwang.huang@gmail.com

<sup>1</sup> Center for the Study of Applied Psychology, Key Laboratory of Mental Health and Cognitive Science of Guangdong Province, School of Psychology, South China Normal University, Guangzhou 510631, China

<sup>2</sup> Department of Radiology, Guangdong Academy of Medical Sciences, Guangdong General Hospital, Guangzhou, China

<sup>3</sup> Center for Cognition and Brain Disorders, Hangzhou Normal University, Hangzhou 310015, China

<sup>4</sup> Zhejiang Key Laboratory for Research in Assessment of Cognitive Impairments, Hangzhou 310015, China

<sup>5</sup> Department of Psychology and Program in Molecular, Cellular, and Integrative Neurosciences, Colorado State University, Fort Collins, CO, USA

## Abbreviation

|      |                          |
|------|--------------------------|
| mPFC | Medial prefrontal cortex |
| SN   | Saliency network         |
| FPN  | Fronto-parietal network  |
| SMN  | Somatomotor network      |
| VN   | Visual network           |
| pCER | Posterior cerebellum     |
| DMN  | Default mode network     |

## Introduction

Parkinson's disease (PD) is a progressive neurodegenerative disorder characterized by a variety of motor and non-motor abnormalities, affecting motor behaviors, executive function, episodic memory, attention, and mood (Pont-Sunyer et al. 2014). PD is caused by a significant reduction of dopaminergic cells in the substantia nigra pars compacta (Fearnley and Lees 1991) which leads to dopamine deficiency in mesencephalic structures and the basal ganglia, and finally affects the neocortex as evident from neuropathologic studies (Hawkes et al. 2009; Braak et al. 2003; Jucker and Walker 2013). Such wide spread dysfunction also affects functional connectivity (FC) between brain regions, as found in numerous PD-related resting-state BOLD fMRI (R-fMRI) studies demonstrating abnormal functional interactions within the cortico-striato-thalamic-cortical loop (Helmich et al. 2010; Göttlich et al. 2013; Kurani et al. 2015). Recently, a growing body of recent R-fMRI studies using complex network measures have shown that PD may induce abnormal topology in brain functional networks. The networks affected include those within the triple network model - the default mode network (DMN), the salience network (SN) and the executive/fronto-parietal network (FPN)- as well as others including motor and visual networks (Skidmore et al. 2011; Baggio et al. 2014; Lebedev et al. 2014; Luo et al. 2015; Tinaz et al. 2015; Putcha et al. 2015; Gorges et al. 2015). These findings suggest that the effects of PD may not be limited to striatal network-related dysfunction, and that a systematic characterization of whole-brain functional networks may provide useful new insights into PD.

Whole-brain functional networks can be characterized in terms of fundamental principles of topological organization, including the characteristic of modularity (Bullmore and Sporns 2009; Bullmore and Bassett 2011). Modularity can be briefly described as dividing the whole-brain functional networks into a set of modules, each module consisting of nodes with dense intra-modular connectivity and relatively sparse inter-modular connectivity with nodes in other modules. Commonly used topological measures are described in Table 2, including the clustering coefficient (prevalence of clustered connectivity around individual nodes, a measure of segregation) and characteristic path length (mean connectivity

weight between nodes, a measure of integration). Usually, modules have the topological property of small-worldness, defined as high clustering within modules and sparse but direct connections between modules. Small-worldness is advantageous for the nervous system, because densely intra-connected brain regions (high clustering) within the same module can support effective segregated processing for specialized functions (i.e. motor functions), while sparsely but directly inter-connected brain regions (short characteristic path length) distributed across modules can support effective globally integrated processing underlying more general functions (i.e. executive functions) Sporns and Zwi (2004). These topological parameters are also useful for characterizing modules whose topological properties are not fully represented by whole-brain measures of topological organization (He et al. 2009). In addition, topological measures such as nodal strength and participation coefficient (Bullmore and Bassett 2011) can provide additional information about intra- and inter-modular connectivity at the nodal level.

Neural topological organization may be impaired by neurological diseases (Vaessen et al. 2013; Alexander-Bloch et al. 2010; Dubbelink et al. 2013). For example, Dubbelink et al. (2013) showed that brain networks in Alzheimer's disease patients were more randomly organized than in controls. In addition, lower intra-modular and inter-modular FC has been reported in Alzheimer's disease (de Haan et al. 2012; Dai et al. 2014), providing better understanding of the underlying pathophysiological mechanisms (Dubbelink et al. 2013).

Parkinson's disease may also distort functional networks. Decreased global and local efficiency (Skidmore et al. 2011; Göttlich et al. 2013; Luo et al. 2015), changed nodal degree (Göttlich et al. 2013), and re-distributed nodal centralities (hubs) (Baggio et al. 2014) have been reported in PD patients compared to controls. A significantly increased modularity index in PD patients with mild cognitive impairment has also been reported (Baggio et al. 2014; Lebedev et al. 2014). Moreover, two studies (Baggio et al. 2014; Putcha et al. 2015) selected three core modules - DMN, SN, and FPN - to explore their intra- and inter-modular FCs. They found that PD patients showed reduced FC within DMN and SN, and between SN and the other two modules: DMN and FPN. In addition, another study reported lower FC within the sensorimotor network in PD patients (Luo et al. 2015). However, most of previous module-related studies were limited to identification of modules containing abnormal regions (Göttlich et al. 2013; Lebedev et al. 2014) or to simply estimating the number of modules (Baggio et al. 2014). Although altered inter-modular FCs were found between certain modules in PD patients, little is known about how the disease affects other inter-modular interactions during the resting state. No studies have reported intra-modular topological organization in PD patients and little is known about how the severity of damage to each module is ordered in PD patients.

In this study, we examined the topological organization of brain functional networks in PD patients and healthy controls, across global, intermediate modular and nodal levels of analysis, by using R-fMRI and graph theory. We first identified the modules present in whole-brain functional networks in PD and controls. We then examined if intra-modular topology and inter-modular functional connections were altered in early-to-mid stage PD patients off medication, and if module-based topological parameters could provide a potential biomarker for PD identification.

## Materials and methods

### Subjects

Thirty-six idiopathic PD patients were recruited in this study. All of the patients were diagnosed by two experienced neurologists (LW and YZ) who have more than 10 years of diagnostic experience in movement disorders. Diagnosis was according to the clinical diagnostic criteria of the UK Parkinson's Disease Society Brain Bank. For each patient, the severity of clinical motor symptoms was assessed according to the Hoehn and Yahr (H-Y) scale (Hoehn and Yahr 1998) and the Unified Parkinson's Disease Rating Scale III (UPDRS III). The inclusion criterion for the PD patients was early-to-mid clinical motor stage (an H-Y stage I or II). The exclusion criteria were as follows: (a) atypical PD syndromes due to drugs or metabolic disorders, encephalitis, or other disease showing similar initial symptoms (i.e., multiple system atrophy and progressive supranuclear palsy); (b) presence of dementia as determined by the clinical evaluation; (c) history of significant neurological disorder or substance abuse or brain injury; and (d) MRI findings of severe abnormalities or lesions including intracranial space-occupying lesions, such as tumors, parasites, or vascular malformations. The diagnostic period for the PD patients was from November 2011 to June 2013 in the Guangdong General Hospital in Guangzhou. For each patient, in order to minimize the impact of antiparkinson medication and induce a relatively hypodopaminergic state (that is, off state), antiparkinson medications had not been taken within 24 h prior to the MRI scanning. Four PD patients were excluded due to excessive head motion (three), failure of normalization (one subject due to abnormal prefrontal morphology) or falling asleep (zero) during the fMRI scan. Thus, thirty-two PD patients (13 M/19 F, age =  $59.3 \pm 10.3$  years old) were retained for the following analysis. In addition, we recruited thirty-one healthy subjects as the controls (12 M/19 F, age =  $61.9 \pm 10.3$  years old). No control subject had any history of psychiatric or neurological disorder or brain injury.

For all of the enrolled subjects, we assessed their general cognitive ability by using the Chinese version of the Mini-

Mental State Examination (MMSE). Table 1 lists the demographic and clinical characteristics for all the subjects. The protocol for the present study was approved by the Institutional Review Board of the Guangdong General Hospital. Written informed consent was obtained from the healthy subjects and from the legal surrogates of the patients.

### Image acquisition

All MRI data were acquired on a 3 T GE MRI scanner with a standard 8-channel phased-array receiver-only head coil at the Guangdong General Hospital. For each subject, we acquired R-fMRI data with a gradient-echo EPI sequence (reception time = 2000 ms, echo time = 30 ms, flip angle =  $80^\circ$ , matrix size =  $64 \times 64$ , field of view =  $256 \times 256$  mm<sup>2</sup>, voxel size =  $3.75 \times 3.75 \times 4$  mm<sup>3</sup>, slice thickness/gap = 4 mm/1 mm, 30 axial slices covering the whole brain, and 186 volumes). During the R-fMRI scanning, each subject was asked to close their eyes and to simply lie quietly in the scanner as motionless as possible. After completion of the fMRI scan, each subject was requested to report whether he or she fell asleep or not. We also acquired high-resolution brain structural images for each subject using a T1-weighted 3D rapid interference phase gradient echo flip recovery pulse sequence (TR/TE = 8.4/3.3 ms, FA =  $13^\circ$ , FOV =  $240 \times 240$  mm<sup>2</sup>, matrix size =  $256 \times 256$ , slice thickness = 1 mm, voxel size =  $0.94 \times 0.94 \times 1$  mm<sup>3</sup>, and 146 sagittal slices covering the whole-brain). The high resolution scan was also used to check for brain structural anomalies, including atrophies, cysts, and tumors, as described in the Subjects section, above.

### Data preprocessing

Functional images were preprocessed using SPM8 (<http://www.fil.ion.ucl.ac.uk/spm>). For each subject, we first discarded the first 10 volumes, then performed slice timing correction for the

**Table 1** Demographics and clinical characteristics of the patients with Parkinson disease (PD) and the healthy controls (HC) in this study. Abbreviations: MMSE - Mini-Mental State Examination; UPDRS III - Unified Parkinson's Disease Rating Scale III

| Parameter                  | PD ( <i>n</i> = 32) | HC ( <i>n</i> = 31) | <i>p</i> -value    |
|----------------------------|---------------------|---------------------|--------------------|
| Mean age (years old)       | 59.30 ± 10.30       | 61.90 ± 10.20       | 0.319 <sup>a</sup> |
| Gender                     | 13 M/19 F           | 12 M/19F            | 0.877 <sup>b</sup> |
| MMSE                       | 27.10 ± 2.64        | 28.52 ± 1.85        | 0.023 <sup>a</sup> |
| Disease duration (years)   | 3.30 ± 2.70         | N/A                 | N/A                |
| Hoehn and Yahr (H-Y) score | 2.13 ± 0.67         | N/A                 | N/A                |
| UPDRS III                  | 29.34 ± 10.68       | N/A                 | N/A                |

<sup>a</sup> The *p*-value was obtained from a two-sample two-tailed *t*-test

<sup>b</sup> The *p*-value was estimated obtained from a two-tailed Pearson's  $\chi^2$ -test  
N/A not applicable

remaining 176 volumes to account for the acquisition time delay between different slices and realigned to the first volume for head-motion correction. The images were normalized to the MNI space using an optimized 12-parameter affine transformation and nonlinear deformations (Ashburner and Friston 2000). Then we performed signal linear detrending, temporal band-pass filtering (0.01–0.08 Hz), and removal of nuisance covariates (signals of white matter and cerebrospinal fluid of whole-brain, head-motion profiles). Although spatial smoothing is typically performed in fMRI studies to increase signal-noise-ratio and to improve signal normality, we skipped this step because it may introduce spurious local connections that are unrelated to real connectivity (Zuo et al. 2012). In this study, the global signal was not regressed out due to controversy over the appropriateness of this procedure for preprocessing R-fMRI data (Fox et al. 2009; Murphy et al. 2009).

Recent studies (Satterthwaite et al. 2012; Van Dijk et al. 2012; Power et al. 2015) have highlighted the influence of head-motion on topological parameters of resting-state functional network. In order to minimize the effects of head-motion in the R-fMRI analysis as much as possible, we adopted the following strategies. First, we excluded subjects if their head motion was greater than a translation  $>2$  mm in any plane or rotation  $>2^\circ$  in any direction as measured during realignment. Second, we estimated several summary measures (maximum, root mean square, and mean frame-wise displacement) from the head-motion profiles (3 translations and 3 rotations) derived from realignment. Statistical comparison showed no significant between-group difference in any of these measures ( $p > 0.05$ ). Third, in addition to the conventional six-parameter head-motion correction realignment, we also applied Friston's 24-parameter approach (Friston et al. 1996) to remove head-motion effects from the time series of each voxel. A previous study (Yan et al. 2013) found that this is an efficient strategy for reducing the residual effects of head-motion on network analysis. Finally, we took the summary measures of head-motion as covariates during statistical comparisons.

### Construction of weighted brain networks

Brain functional networks are defined as a collection of nodes linked by edges where nodes correspond to brain regions and edges to inter-nodal connections. To define the nodes, we adopted a method developed by Zalesky et al. (2010) to randomly divide the brain into 1,024 equal volume cortical and sub-cortical regions (brain partition see Fig. S1 and Fig. S2). Here we included the cerebellum as it may play a role in the pathophysiology of PD (Wu and Hallett 2013). To measure the inter-nodal connection, we first calculated Pearson's correlation coefficients between each pair of nodes and significance level (i.e.,  $p$  value) of a given inter-regional correlation. Then we generated a weighted  $1,024 \times 1,024$  correlation

matrix and the corresponding  $p$  value matrix for each subject. To de-noise spurious correlations, we retained only those correlations whose corresponding  $p$  values passed a statistical threshold of  $p < 0.05$  (Bonferroni correction); otherwise, we set the correlation to zero (Cruse et al. 2011). By taking the remaining Pearson's coefficients as edge weights, we obtained a weighted  $1024 \times 1024$  FC matrix, which was used to conduct the subsequent analysis for each subject. Additionally, we discarded negative correlations due to ambiguities in their interpretation and their detrimental effects on test-retest reliability (Achard and Bullmore 2007; Wang et al. 2011).

### Modular analysis

#### *Identification and partitioning of modules*

Functional network modules are defined as sets of nodes that are densely linked with each other and less so with other nodes in the network (that is, other modules). The modularity measure,  $Q$ , quantifies the difference between the weight of intra-modular edges in the real network and that of random networks (Newman 2004). To maximize  $Q$  value resulting in the best possible modular partitions, we used the spectral optimization algorithm proposed by Newman (2006) and reported the maximized value of  $Q$  for the brain networks (for the mathematical definition of  $Q$  see Table 2). Higher values of  $Q$  indicate greater functional specialization of a brain network.

For both the PD patients and the controls, we estimated their most representative group-level modular partitions. First, we only retained a given edge weight if it appeared in no less than 80 % of subjects. Then we averaged each edge weight across individuals to obtain the group-averaged weighted FC matrix for each group. Second, based on this group-mean FC matrix, we used nonparametric sparsification method (Foti et al. 2011) to extract two backbone networks for each group. In this calculation, we selected those locally significant edges which could not be explained by random variations to form the backbone networks. Finally, the two backbone networks were used to identify the modular partition that captured underlying common connectivity patterns for all subjects in the present study.

#### *Modular network parameters*

For each subject, we analyzed PD-related alterations of modular network organization on two-levels: module-level and node-level. At the module-level, we determined 1) intra-modular small-world attributes within each module, including clustering coefficient ( $C_p$ ), characteristic path length ( $L_p$ ), normalized clustering coefficient ( $\gamma$ ), and normalized characteristic path length ( $\lambda$ ); 2) inter-modular FC strength by summarizing all inter-nodal FCs across pairs of modules; and 3) the centrality of modules contributing to the whole-brain network. We adopted a two-step analysis. First, for the quality analysis, we followed the method

**Table 2** Formulas for topological parameters of a brain network. Their descriptions and definitions can also be found in Rubinov and Sporns (2010)

| Modular parameter                    | Definition  | Note  |
|--------------------------------------|---|---|
| Modularity                           | $Q = \frac{1}{2m} \sum_{ij} \left( A_{ij} - \frac{k_i k_j}{2m} \right) \delta_{s_i s_j}$                  | Here $m$ is the total number of edges for a network. $k_i$ and $k_j$ are the degrees of nodes $i$ and $j$ . $A_{ij}$ is the number of edges between nodes $i$ and $j$ . $k_i k_j / 2m$ is the probability that there would be an edge between $i$ and $j$ . $\delta_{s_i s_j}$ is the Kronecker delta. $Q$ quantifies the difference between the weight of intra-modular links of the actual network and that of random networks in which connections are weighted at random. |
| Clustering coefficient               | $C_p = \frac{1}{N} \sum_{i \in N} \frac{\sum_{j, h \in N} (w_{ij} w_{ih} w_{jh})^{1/3}}{k_i (k_i - 1)}$   | For a weighted network or a module with $N$ nodes, $w_{ij}$ is the edge weight between node $i$ and $j$ . $k_i$ is the degree of node $i$ . $C_p$ is the mean of the clustering coefficient over all nodes and indicates the extent of local interconnectivity or cliquishness in a network or a module.  |
| Characteristic path length           | $L_p = N(N-1) \sum_{i=1}^N \sum_{j \neq i}^N 1/l_{ij}$  | For a weighted network or a module with $N$ nodes, $l_{ij}$ is the weighted characteristic path length between nodes $i$ and $j$ . $L_p$ is the mean of the characteristic path length over all nodes and indicates the extent of overall routing efficiency of a network or a module.  |
| Normalized nodal strength            | $K_i^n = K_{S_i} / (N_{\text{mod}} - 1)$  | $K_{S_i}$ is the weighted connections of node $i$ to other nodes. $N_{\text{mod}}$ is the number of modules for each subject. $K_i^n$ quantifies the extent of a region's connections within the same modules.  |
| Normalized participation coefficient | $PC_i^n = \frac{N_{\text{mod}}}{(N_{\text{mod}} - 1)} \left[ 1 - \sum_{s \in M} (k_{is} / k_i)^2 \right]$ | $M$ is the set of modules. $K_{is}$ is the number of links of node $i$ to other nodes in module $s$ . $k_i$ is the total weight of node $i$ . $N_{\text{mod}}$ is the number of modules for each subject. $PC_i^n$ quantifies the extent of a region's connections to other modules.  |

described in Achard et al. (2006) to explore the impact of an isolated module attack on the whole brain network. For this calculation, we eliminated each module (including all its nodes and related connections) in turn, re-estimated the mean characteristic path length in its absence, and estimated the percent change in characteristic path length,  $\Delta L_p / L_p$  ( $L_p$  after elimination -  $L_p$  before elimination) /  $L_p$  before elimination). For a given module, a higher absolute value of  $\Delta L_p / L_p$  likely reflects a greater impact of that modular attack on the whole-brain network topology. Second, for the quantitative analysis, we re-compared the between-group differences in  $C_p$  and in  $L_p$  for the residual networks between the PD patients and the controls when each module was removed one-by-one. At the node level, we calculated two indices, normalized nodal strength ( $K_i^n$ ) and normalized participation coefficient ( $PC_i^n$ ), for all nodes to reflect their roles in dominating intra-modular and coordinating inter-modular FC, respectively (Guimera and Amaral 2005).  $K_i^n$  quantifies functional connectivity strength of node  $i$  to other nodes within module and  $PC_i^n$  measures how 'well-distributed' the edges of node  $i$  are among different modules. All of the parameters mentioned above are listed in Table 2. Of note, all of the calculations were in reference to the group-level module partition of the healthy controls (see 'Identification and partitioning of modules').

### Statistical analysis

We compared the modularity  $Q$  obtained from the real data with that of 100 randomly-generated networks which were created by a topological rewiring procedure (Sporns, 2011).

We defined  $\eta = (Q - Q_{\text{rand}}) / Q_{\text{std}}$ , where  $Q$  is the modularity of the real brain network, and  $Q_{\text{rand}}$  ( $Q_{\text{std}}$ ) is the mean (standard deviation) of modularity over all randomized networks (Chen et al. 2011b).

A nonparametric permutation test was applied to determine the statistical significance of the between-group difference in each of the modular network parameters ( $Q$ ,  $C_p$ ,  $L_p$ ,  $\lambda$ ,  $\gamma$ , inter-modular FC,  $K_i^n$ , and  $PC_i^n$ ). For a given parameter, we initially calculated the difference in its mean values between the PD and control groups, and then estimated the null hypothesis that the observed between-group difference could occur by chance. To this end, we randomly reallocated all the values of this parameter into two groups and recomputed the difference in the mean values between the two randomized groups. This randomization procedure was repeated 10,000 times in order to obtain an empirical distribution of the difference. The 95th percentile distribution was used as the critical value for a two-tailed test of the null hypothesis with 5 % probability of type-I error (or false positive). In the calculations, we regressed out the effects of confounding factors, including age, gender, age-gender interaction, and summary of head motion. The false discovery rate (FDR) method (Benjamini and Hochberg 1995) was used to correct for multiple comparisons when needed.

### Brain-behavior correlations

A multiple linear regression analysis was used to assess the relationship between each of the modular parameters and

clinical variables (MMSE, H-Y, UPDRS III, and disease duration) in the PD patients. Age, gender, age-gender interaction, and the head motion summary parameters were treated as confounding factors.

### ROC analysis

We plotted receiver operating characteristic (ROC) curves to determine whether the modular network parameters might serve as biomarkers for discriminating PD patients from controls. An ROC curve is a graphical plot that illustrates the performance of a binary classifier system as the discrimination threshold is varied. The curve is created by plotting the true positive rate (TPR) against the false positive rate (FPR) at various threshold settings. The true-positive rate is known as sensitivity in signal detection or in machine learning. Detection is calculated by evaluating the significance of the area under the ROC curve (AUC).

The procedure for generating ROC curves was as follows (Chen et al. 2011a; Chen et al. 2013). We took each modular network parameter as a one-dimensional feature and selected different thresholds to categorize each subject into either the PD group or the control group. At a given threshold, the TPR (i.e., sensitivity) measures the fraction of subjects that were correctly identified as PD patients, and the true negative rate (i.e., specificity or 1-FPR) evaluates the fraction of subjects that were correctly identified as healthy controls. A so-called ‘cut-off point’ was determined by simultaneously optimizing sensitivity and specificity. All the steps were processed using publicly available MATLAB code (<http://www.mathworks.com/matlabcentral/fileexchange/199500-roc-curve>; Giuseppe Cardillo). The accuracy, sensitivity (or true positive rate, TPR), and specificity (or 1-false positive rate, 1-FPR) were reported.

## Results

### Demographic and neuropsychological information

Table 1 shows no significant differences either in gender ( $p = 0.877$ ) or in age ( $p = 0.320$ ) between the PD patients and the controls. The MMSE scores of PD patients were significantly lower compared to the controls ( $p = 0.023$ ). No significant differences in head motion summary measures were found between the PD patients and the controls (Table S1 in supplementary materials).

### Modular network organization

We estimated the topological parameters of the whole-brain functional network for each subject in this study. As expected, both groups exhibited high  $Q$  values compared with their corresponding 100 random networks ( $\eta_{\min} = 45.9$ ,  $p_{PD} < 10^{-10}$ ;

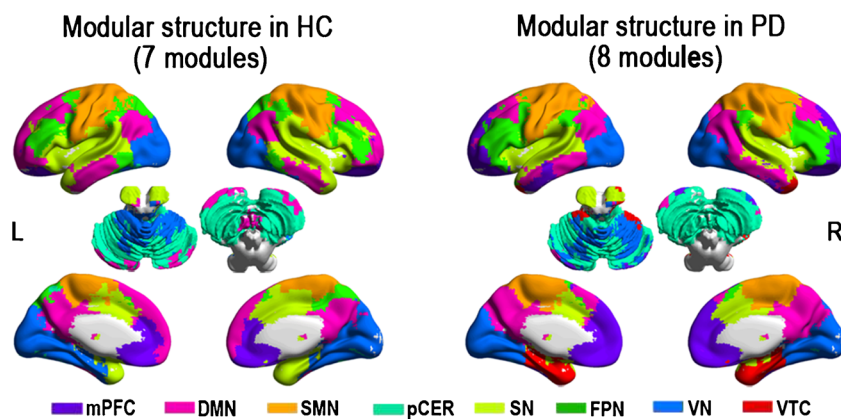
$\eta_{\min} = 44.6$ ,  $p_{\text{controls}} < 10^{-10}$ ). No significant between-group difference was found either in  $Q$  ( $p = 0.502$ ) or in the small-worldness  $\sigma$  ( $p = 0.790$ ) (for statistics of global parameters in the whole-brain networks see Table S2).

Figure 1 shows seven modules in the controls ( $Q_{\text{group}} = 0.569$ ,  $\eta = 221.1$ ) that were identified from the group-averaged FC matrix, including the medial prefrontal cortex (mPFC), salience network (SN), fronto-parietal network (FPN), somatomotor network (SMN), visual network (VN), posterior cerebellum (pCER), and default mode network (DMN). Of note, the borders of this network were not identical to those identified as DMN in other studies. The areas identified here were primarily the posterior regions of the conventional DMN, and in addition included a few regions located in cerebellum. For the PD patients, we identified eight modules ( $Q_{\text{group}} = 0.565$ ,  $\eta = 191.5$ ) which were quite similar to those in the controls (normalized mutual information = 0.63). The visual network (depicted in blue in Fig. 1) identified in the controls corresponded to two modules in the patients (depicted in red and blue in Fig. 1), while the mPFC network (depicted in purple in Fig. 1) occupied a larger area in the patients.

We also calculated intra-modular topological parameters as shown in Fig. 2a. Compared to the controls, the PD patients exhibited a significantly increased characteristic path length ( $L_p$ ) within four modules: the mPFC ( $p = 0.020$ ), salience ( $p = 0.012$ ), fronto-parietal ( $p = 0.028$ ), and somatomotor ( $p = 0.028$ ) (FDR correction,  $q = 0.05$ ) (Table S3).  $C_p$  was significantly decreased in three modules, VN, SN, and SMN (uncorrected), in PD compared with controls (Table S3). None of the other three parameters ( $\gamma$ ,  $\lambda$ , and  $\sigma$ ) showed significant between-group difference within any of the modules.

We then calculated inter-modular FC as shown in Fig. 2b and Table S4. We found significantly decreased inter-modular FC between the mPFC and the other three modules, SN ( $p = 0.001$ ), SMN ( $p = 0.002$ ), and VN ( $p = 0.004$ ), in the patients compared to the controls (FDR correction,  $q = 0.05$ ). In addition, we found the inter-modular FC between mPFC and FPN, between mPFC and pCER, and between SN and VN also were significantly decreased in the patients compared to the controls (uncorrected) (Table S3).

Table 3 (first four columns) shows the relative change in characteristic path length ( $L_p$ ) for both groups. The  $\Delta L_p$  was the difference in  $L_p$  between the whole-brain functional network and the residual networks after a module being removed. For each group, the percentage change in ( $\Delta L_p/L_p$ ) was estimated after individually eliminating each module as described in the Method section and by Achard et al. (2006). Disregarding the direction of change, for the controls, the most central modules in descending order were DMN, SN, pCER, SMN, mPFC, FPN, and VN ( $\Delta L_p/L_p$  was  $-0.017$ ,  $-0.010$ ,  $-0.009$ ,  $0.007$ ,  $-0.006$ ,  $-0.001$ , and  $-0.0001$ ,



**Fig. 1** Modular organization in the healthy controls (left) and the patients with Parkinson's disease (PD) (right). Seven group-level modules were found in the whole-brain functional network of the controls ( $Q = 0.569$ ): the medial prefrontal cortex (mPFC, in purple), default mode network (DMN, magenta), somatomotor network (SMN, orange), posterior

cerebellum (pCER, turquoise), salience network (SN, yellow), fronto-parietal network (FPN, green), and visual network (VN, blue) (left in the figure). Eight group-level modules were detected in the whole-brain functional network of the PD patients, including an additional module the ventral temporal cortex (VTC, red) not identified in the controls

respectively). Whereas for the PD patients, this order was slightly different: SN, DMN, mPFC, pCER, VN, FPN, and SMN ( $\Delta L_p/L_p$  was  $-0.014, -0.008, -0.007, -0.003, -0.003, 0.001,$  and  $0.002,$  respectively).

Figure 3 shows the between-group difference in characteristic path length in residual brain networks contrasted to the whole-brain networks. In the whole-brain networks, we found that compared to the controls, the PD patients showed significantly decreased clustering coefficient ( $p = 0.026$ ) and increased characteristic path length ( $p = 0.037$ ). When any module was removed from the whole-brain networks, in each of the residual networks, the PD patients still showed significantly decreased clustering coefficients (FDR correction,  $q = 0.05$ ) but conserved characteristic path length (FDR correction,  $q = 0.05$ ) compared to the controls (see latter six columns in Table 3).

Figure 4 shows the PD-related alterations in the nodal roles in terms of the intra- and inter-modular FC, as indexed by normalized strength  $K_i^n$  and  $PC_i^n$ , respectively. Figure 4a shows that the PD patients had significantly altered  $K_i^n$  in a total of 544 nodes compared to the controls (FDR correction,  $q = 0.05$ ). Among these nodes, 518 (accounting for  $518/544 = 95.2\%$  of 544 nodes) showed significantly decreased  $K_i^n$  in the patients, which were unevenly distributed in five modules, DMN (223/544 or 41.0%), SN (214/544 or 39.3%), FPN (52/544 or 13.2%), VN (23/544 or 4.2%), and SMN (6/544 or 1.1%). The remaining 26 nodes (less than 5% of 544 nodes) showed significantly increased  $K_i^n$  in the patients and were located in both the mPFC (6/544 or 1.1%) and FPN (20/544 or 3.7%). As for  $PC_i^n$ , we found 7 nodes, located in DMN, showed uniformly significantly increased  $PC_i^n$  in the PD patients compared to the controls (Fig. 4b).

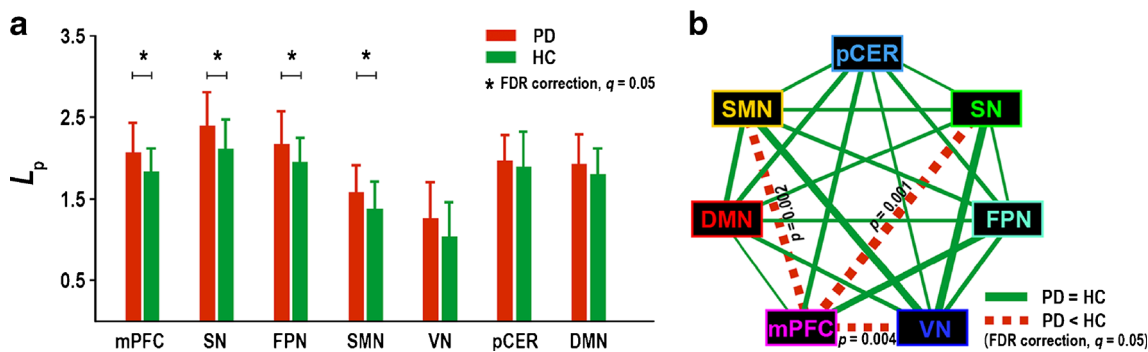


**Fig. 2** Intra-modular small-world attributes and inter-modular functional connectivity (FC) for both the PD patients and the healthy controls. **a** Within four modules, mPFC, SN, FPN, and SMN.  $L_p$  showed significant between-group difference (\* FDR correction,  $q = 0.05$ ). **b** FC between pairs of modules. The PD patients showed significantly decreased inter-modular FC compared to the controls (FDR correction,  $q = 0.05$ ) between mPFC and the other three modules, SN, SMN, and VN. Dashed red lines

indicate significantly decreased inter-modular FC in the PD patients compared to the controls. Solid green lines refer to non-significant between-group difference in the inter-modular FCs. Line widths are inversely proportional to the  $p$ -value of between-group differences in the inter-modular FC. Full names of abbreviations for different modules were given in Fig. 1

**Table 3** Modular centrality for both the patients with Parkinson disease (PD) and the healthy controls (HC) in this study.  $\widetilde{DMN}$  indicates the residual brain network when the DMN module was removed from the whole-brain network (WBN)

| Residual brain network | $L_p$ |        | $\Delta L_p/L_p$ |         | $C_p$         |               |                 | $L_p$         |               |                 |
|------------------------|-------|--------|------------------|---------|---------------|---------------|-----------------|---------------|---------------|-----------------|
|                        | PD    | HC     | PD               | HC      | PD            | HC            | <i>p</i> -value | PD            | HC            | <i>p</i> -value |
| WBN                    | -     | -      | -                | -       | 0.318 ± 0.048 | 0.365 ± 0.088 | 0.026 ↓**       | 3.048 ± 0.329 | 2.819 ± 0.445 | 0.037 ↑**       |
| $\widetilde{SN}$       | 3.007 | -0.014 | 2.816            | -0.010  | 0.321 ± 0.049 | 0.369 ± 0.088 | 0.024 ↓**       | 3.026 ± 0.338 | 2.802 ± 0.446 | 0.055           |
| $\widetilde{DMN}$      | 3.024 | -0.008 | 2.796            | -0.017  | 0.330 ± 0.045 | 0.375 ± 0.085 | 0.022 ↓**       | 3.007 ± 0.325 | 2.795 ± 0.457 | 0.035 ↑*        |
| $\widetilde{mPFC}$     | 3.026 | -0.007 | 2.827            | -0.006  | 0.322 ± 0.047 | 0.369 ± 0.089 | 0.024 ↓**       | 3.053 ± 0.330 | 2.816 ± 0.453 | 0.045 ↑*        |
| $\widetilde{pCER}$     | 3.038 | -0.003 | 2.817            | -0.009  | 0.318 ± 0.045 | 0.361 ± 0.082 | 0.017 ↓**       | 3.051 ± 0.315 | 2.843 ± 0.425 | 0.027 ↑*        |
| $\widetilde{VN}$       | 3.039 | -0.003 | 2.843            | -0.0001 | 0.324 ± 0.047 | 0.366 ± 0.082 | 0.041 ↓**       | 3.039 ± 0.329 | 2.819 ± 0.423 | 0.039 ↑*        |
| $\widetilde{SMN}$      | 3.051 | 0.001  | 2.864            | 0.007   | 0.325 ± 0.049 | 0.373 ± 0.086 | 0.028 ↓**       | 3.038 ± 0.335 | 2.793 ± 0.443 | 0.046 ↑*        |
| $\widetilde{FPN}$      | 3.053 | 0.002  | 2.840            | -0.001  | 0.324 ± 0.053 | 0.376 ± 0.094 | 0.024 ↓**       | 3.024 ± 0.371 | 2.768 ± 0.463 | 0.033 ↑*        |

Modules were ranked in order of increasing characteristic path length presented in the residual brain network of the PD patients (the first column). The  $L_p$  value in the first and third column were based on mean of all individual's  $L_p$  score.  $\widetilde{DMN}$  indicates the residual brain network when the DMN module was removed from the whole-brain network (WBN).  $C_p$  ( $L_p$ ) is the clustering coefficient (characteristic path length).  $\Delta L_p/L_p$  is the relative change in the characteristic path length for the residual brain network when the WBN was attacked by eliminating a certain module and all of its connections. The larger the absolute value of  $\Delta L_p/L_p$ , the more central of that module in the WBN. The *p*-values indicate between-group comparison (PD vs. HC) of clustering coefficient and characteristic path length in the residual brain networks (10,000 permutations)

\*\*FDR correction,  $q = 0.05$

\*uncorrected,  $p < 0.05$

↓(↑) significant decrease (increase) in PD compared to HC. Abbreviations of modules can be found in Fig. 1

## Brain-behavior relationships

Figure 5a shows the relationships between modular parameters and clinical variables in the PD patients (each symbol ○ in red (green) represents a PD patient (healthy control)). In the mPFC, we observed that the characteristic path length was significantly positively correlated with MMSE score ( $r = 0.423$ ,  $p = 0.05$ ). In the posterior cerebellum, the normalized participation coefficient  $PC_i^n$  was also significantly positively correlated with MMSE score ( $r = 0.425$ ,  $p = 0.049$ ). However, no significant correlation was detected between any of other modular parameters ( $Q$ ,  $C_p$ ,  $\lambda$ ,  $\gamma$ , inter-modular FC, and  $K_i^n$ ) and any of the clinical variables (UPDRS III, H-Y stage, and disease duration) in the patients.

## ROC analysis

We examined the possibility of using modular topological parameters to discriminate the PD patients from the controls based on the ROC curves. Figure 5b plots the ROC curves for the characteristic path length within two modules, SN and SMN, and for the inter-modular FC between mPFC and SN (FDR correction,  $q = 0.05$ ). The intra-modular characteristic path length within the SN and SMN showed significant

classification power in discriminating the PD patients from the controls, with AUC = 0.667 ( $p = 0.007$ ) and 0.653 ( $p = 0.014$ ), sensitivity = 45.2 % and 48.4 %, specificity = 87.5 % and 81.3 %, and accuracy = 66.7 % and 65.1 %, respectively. In addition, we found the inter-modular FC between the mPFC and SN showed the highest power (AUC = 0.700,  $p = 0.001$ ) for the discrimination, with a sensitivity of 61.3 % and a specificity of 81.3 % (accuracy of 71.4 %) (Table S5).

## Discussion

In this study, we explored the modular organization of whole-brain functional networks in PD using graph theory. Our main findings were: (1) the PD patients showed longer characteristic path length and weaker clustering coefficient at global level; (2) modular level analyses found increased intra-modular characteristic path length within four modules (mPFC, SN, FPN, and SMN), and decreased inter-modular FC between mPFC and SN as well as between mPFC and SMN; (3) additional module centrality analyses showed that an 'attack' on any module produced changed between-group differences in characteristic path length in residual brain networks contrasted

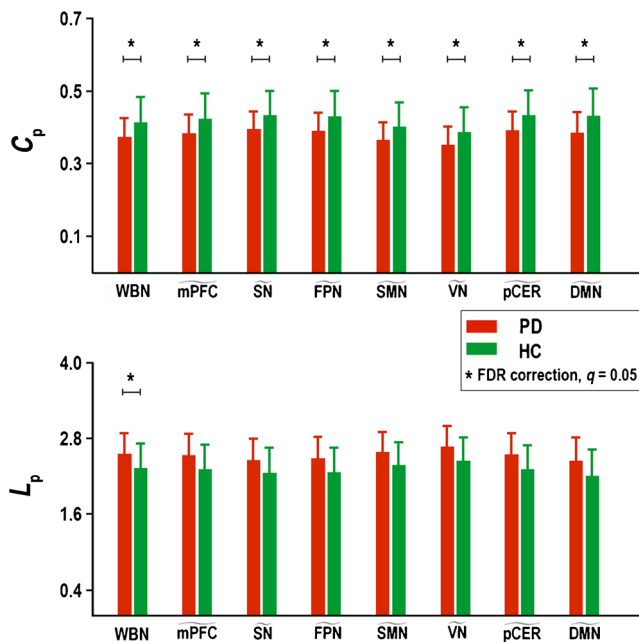


**Fig. 3** Bar plots showing clustering coefficient ( $C_p$ ) and characteristic path length ( $L_p$ ) for both the whole-brain networks (WBN) and the residual brain functional networks for the PD patients and healthy controls (HC). We found that the residual brain networks obtained by removing any individual module showed uniformly significantly decreased  $C_p$  in the PD patients, which was similar to the comparison result of whole-brain network. However, no significant between-group differences in  $L_p$  were found in the residual networks. (\* indicates FDR correction,  $q = 0.05$ ). Here ‘~’ represents the residual brain networks after removing the target module from the WBN. Full names of the abbreviations for different modules can be seen in Fig. 1

with the whole-brain networks; (4) nodes with altered properties were primarily in the DMN and SN; (5) Intra-modular characteristic path length within mPFC showed positive correlation with MMSE score, and (6) FC between mPFC and SN had the highest power to discriminate the PD patients from the controls.

### Modular organization

In this study, we estimated the modularity index of the brain networks for each of the 32 PD patients and 31 controls. We found no significant between-group difference either in modularity index ( $Q$ ) or in small-worldness ( $\sigma$ ) (Table S2). Our findings suggest that subjects in both groups maintain a balance between local specialization and global integration in information processing. Evidence from previous resting-state brain network studies also supported small-worldness and modular structure in PD patients (Göttlich et al. 2013). However, another recent study (Baggio et al. 2014) described significantly increased values of both small-worldness and modularity in PD patients with mild cognitive impairment compared to controls. This discrepancy may be due to the heterogeneity of patients involved in the different studies.

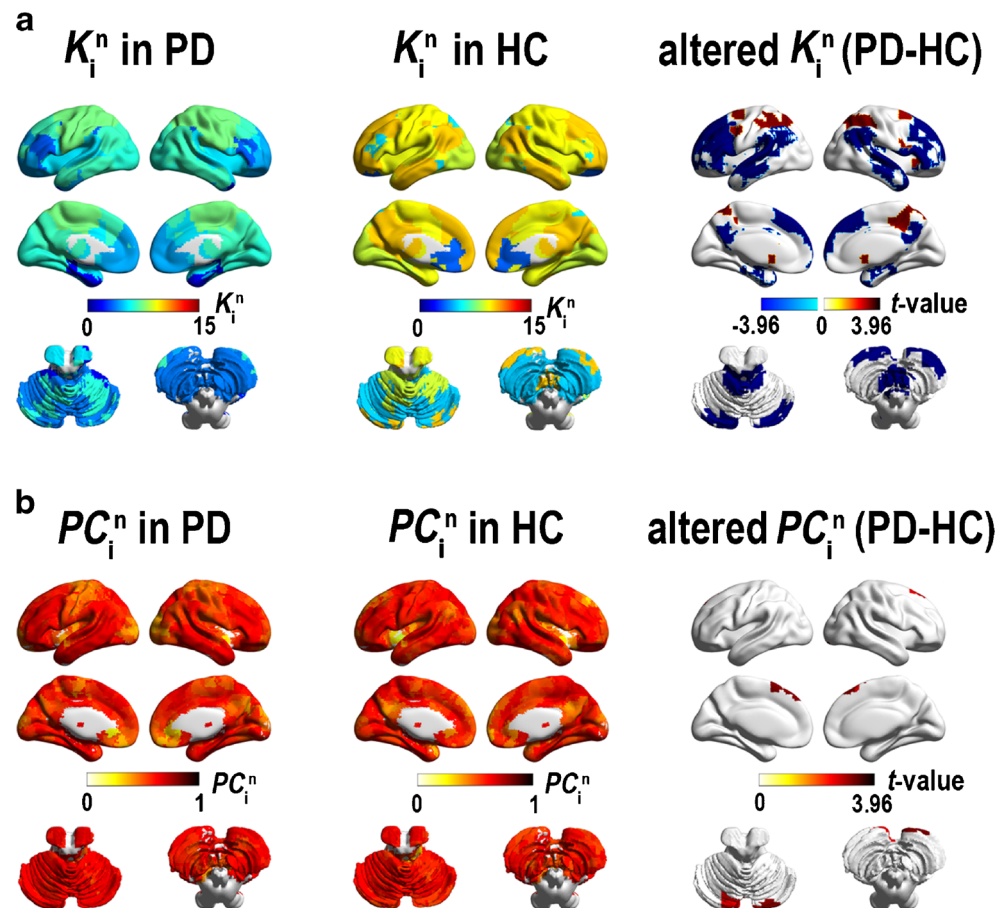
We identified eight and seven modules in the whole-brain functional networks in the Parkinson’s patients and healthy controls, respectively (Fig. 1). This finding is consistent with a recent PD-related study (Göttlich, et al. 2013) that detected seven modules in healthy controls, including sensorimotor, visual, fronto-parietal, and default mode networks. We also noticed that our finding of 8 modules differed from a recent study (Baggio et al. 2014) which identified only four modules in PD patients, including the fronto-parietal, insulo-operculo-striatal, fronto-parieto-parahippocampal, and occipito-temporal modules. This inconsistency may due to different methods used to identify the modules. Baggio et al. (2014) formed the modular partition from the mean brain network across all three groups of subjects, including PD patients with and without cognitive impairment as well as healthy controls, while we identified modules within each subject group independently.

In this study, we also detected between-group difference in module- and node-level topological parameters. In the PD patients, we found longer characteristic path length within four modules, the medial prefrontal cortex (mPFC), salience network (SN), fronto-parietal network (FPN), and somatomotor network (SMN) (Fig. 2a). The mPFC is suggested to be involved in self- reflection, emotion, decision making, and memory (Jenkins and Mitchell 2011; Euston et al. 2012; Somerville et al. 2013). Previous studies detected decreased brain activity in the dorsal mPFC (Cardoso et al. 2009) and decreased cerebral blood flow (rCBF) in the pre-frontal cortex (Borghammer et al. 2012) in PD patients. Our finding of longer characteristic path length indicates a decreased integrity of connections between brain regions within the mPFC in the PD patients.

The SN is believed to contribute to interoceptive and affective processes for capturing biologically and cognitively relevant events (Seeley et al. 2007). The anterior cingulate cortex (ACC) and insula are key regions of SN and are coactivated in response to different forms of salience (Mesulam 1998). In this study, we found the PD patients showed significantly increased characteristic path length in the SN but decreased inter-modular FC between mPFC and SN compared to the controls (Fig. 2b). These results are consistent with several previous PD studies. Kikuchi et al. (2001) detected hypoperfusion in the insula and Christopher et al. (2014) found a decrease of cortical dopamine D2 receptor binding in the SN. Previous studies also reported an impairment of dopamine in the PFC and a deficit of D2 receptors in the insula in PD patients. This suggested the PFC impairments in PD patients may be associated with deficits of verbal fluency performance (Polito et al. 2012) and executive function (Christopher et al. 2014).

The FPN, also called the executive-attention network, is believed to support cognitive control and decision-making (Vincent et al. 2008). We detected alterations in FPN in the

**Fig. 4** Rendering plot of brain regions with significantly changed nodal parameters in the patients with Parkinson disease (PD) compared to the healthy controls (HC) (FDR correction,  $q = 0.05$ ). **a** Normalized nodal strength,  $K_i^n$ , relating to the intra-modular connectivity, **b** Normalized participation coefficient,  $PC_i^n$ , relating to the inter-modular connectivity



PD patients which are in line with several previous studies. Biundo et al. (2013) and Rektorova et al. (2014) detected a decrease of grey matter volume but an increase of cortical thickness in the FPN in PD patients with executive deficits. In addition, Rae et al. (2012) analyzed diffusion fractional anisotropy (FA) and found disrupted white matter integrity in the frontal and parietal lobes in early to mid stage PD patients. A recent R-fMRI study (Lebedev et al. 2014) suggested that the executive performance was positively associated with dorsal fronto-parietal processing in PD patients (Table S6). Thus, we infer that weakened integration, as indicated by a longer characteristic path length within the FPN, may relate to executive function deficits in PD patients.

The SMN is involved in planning and execution of voluntary movements (Ferri et al. 2012). Our finding of abnormal SMN in the PD patients is in line with several previous studies (Boller et al. 1984; Doyon et al. 1997). For PD patients, Boller et al. (1984) reported SMN involvement in visuospatial function, Doyon et al. (1997) found the SMN is related to visuomotor sequence learning, and Wu et al. (2011b) detected significantly increased FC between the preSMA and primary motor cortex. Another R-fMRI study (Pyatigorskaya et al. 2013) suggested that motor abnormalities in PD patients may reflect integration within somatomotor circuits.

We also analyzed the effect of these ‘module lesions’ on whole-brain networks in the PD patients (Table 3 and Fig. 3). For the PD group, the elimination of SN induced the most decreased  $\Delta L_p/L_p$  (-0.014) in the residual brain network, which was followed those of DMN, mPFC, pCER and VN. In contrast, the removal of the SMN was associated with most increased  $\Delta L_p/L_p$  in the residual brain network. The direction of alterations was consistent with the changes in the healthy controls. In terms of between-group comparison, we found attacks on all the modules had significant effects on the  $L_p$  of whole-brain network rather than  $C_p$ . We also considered the roles of brain regions (nodes) in mediating intra- and inter-modular FC by estimating their normalized nodal strength  $K_i^n$  and normalized participation coefficient  $PC_i^n$  (Fig. 4). Higher  $K_i^n$  corresponds to stronger connections to nodes within the same module, and higher  $PC_i^n$  indicates that the node has stronger connections to nodes in other modules. In PD patients, we found that nodes with significantly changed nodal strength were distributed across all modules (Fig. 4a). DMN and SN included the largest numbers of significantly altered nodal connections (with decreased  $K_i^n$ ), suggesting weaker FC within these modules in PD patients compared to the control group. Interestingly, several regions in DMN showed significantly increased  $PC_i^n$ , implying tighter

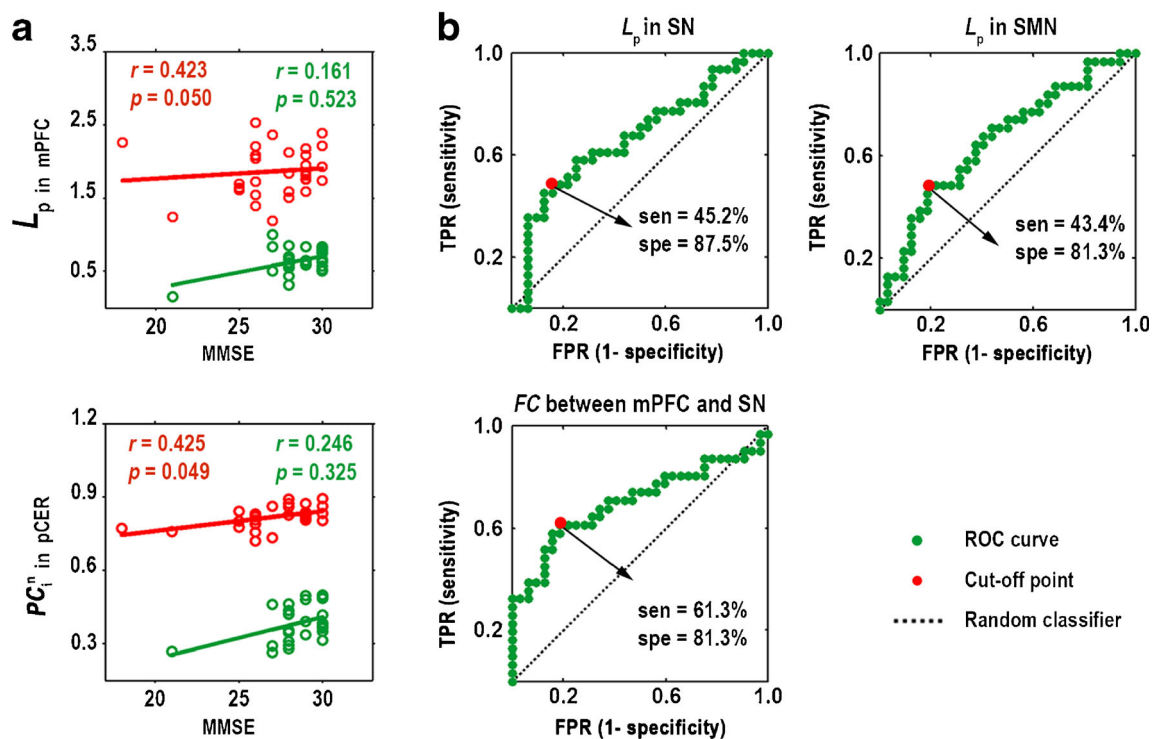


**Fig. 5** Modular parameters in the patients with Parkinson's disease (PD). **a** Relationship between modular parameters ( $L_p$ , characteristic path length;  $PC_n^i$ , normalized participation coefficient) and clinical variables in the PD patients. Each symbol  $\circ$  in red (green) represents a PD patient (healthy control). The  $r$ - and  $p$ -values indicate the correlation and between-group difference level. **b** ROC analysis showing significant classification power of the modular parameters (FDR correction,

$q = 0.05$ ). The red dot indicates the threshold with simultaneously optimized sensitivity and specificity. Abbreviations:  $L_p$ , characteristic path length;  $PC_n^i$ , participation coefficient; mPFC, medial prefrontal cortex; pCER, posterior cerebellum; SMN, somatomotor network; SN, salience network; MMSE, Mini-Mental State Examination; FC, functional connectivity; TPR, true positive rate; FPR, false positive rate; sen, sensitivity; spe, specificity

connections between DMN and other modules in PD patients compared to the controls (Fig. 4b). The DMN has been suggested to be involved in self-referential and emotional processes (Raichle and Snyder 2007; Damoiseaux et al. 2008). A previous R-fMRI study (Tessitore et al. 2012) showed significantly decreased FC within the DMN in PD patients which may hinder normal cognition or executive performance (van Eimeren et al. 2009).

### Brain-behavioral relationship

We observed that characteristic path length in the mPFC was significantly positively correlated with MMSE score in the patients (Fig. 5a). However, we detected no significant correlation between any of modular parameters and any of motor-related clinical variables (i.e., UPDRS III and H-Y) in the PD patients. Thus, we speculate that motor and cognitive impairments in PD patients may have different underlying pathophysiological mechanisms (Dubbelink et al. 2013).

### ROC analysis

In this study, we found that inter-modular FC between the mPFC and SN had the highest classification accuracy at

71.4 % (with 61.3 % sensitivity and 81.3 % specificity) in distinguishing the PD patients from the controls. We also found that characteristic path length within the SN and SMN showed high classification power to distinguish PD patients from controls, with an accuracy of 66.7 % and 65.1 % respectively (Fig 5b). A previous study (Long et al. 2012) reported effective differentiation of PD patients from controls by combining multiple MR imaging modalities. This suggests it may be beneficial to combine multiple parameters to achieving better classification. Although classification accuracy in this study was not very high, the specificity score of  $>80$  % may highlight a significant power of inter-modular FC for distinguishing PD patients (Radebaugh and Khachaturian 1998). The lower sensitivity score of  $<80$  % in current findings may possibly due to using a one-dimensional parameter for the classifier. Future studies can improve classification accuracy by employing more sophisticated methods (e.g., multivariate pattern analysis) and combining multi-level and multi-modal imaging methods.

### Limitations

The current study has several limitations. First, we normalized the functional data to the SPM EPI template which may affect the

accuracy of image transformation. A better way for normalization may be performed using deformation fields generated during tissue segmentation of anatomical data or using the DARTEL (diffeomorphic anatomical registration through exponential Lie algebra) approach (Ashburner, 2007), a fast diffeomorphic image registration algorithm. Second, we adopted the positive Pearson's correlations but discarded negative correlations to build brain FC networks, which may also bias the results. Further studies should offer more evidence by constructing brain functional networks based on both positive and negative correlations. Third, brain functional modules may spatially overlap (Wu et al. 2011a) or contain several sub-components (Chen et al. 2008), which were not considered in this study. Further studies are needed to explore the overlapping and hierarchical modular organization of brain functional networks in PD. Fourth, although the PD patients in this study were restricted to the early-to-mid clinical motor stage, their heterogeneity may have influenced the network topology. A previous study (Pont-Sunyer et al. 2014) indicated that PD subtypes identified on the basis of motor impairment were accompanied by non-motor deficits ranging from mood disorders (e.g., depression) to cognitive abnormalities (e.g., executive dysfunction). Thus, PD patients with different combinations of motor and non-motor impairments may be characterized by different changes in brain functional organization. It would be interesting to delineate specific subtype-related brain network reorganization in the future following a detailed assessment of motor, cognitive, and affective symptoms. Finally, most of the PD patients were taking dopaminergic medications. Although we wanted to study drug-naïve individuals to exclude the effects of dopaminergic medication, we cannot exclude the effect of medication on network analysis.

In conclusion, we detected altered modular organization in intrinsic brain functional networks in patients suffering from early-to-mid stage Parkinson's disease off medication. Through analyzing modular parameters, we found abnormal intra- and inter-modular topological parameters across executive, emotional, and motor-related modules in PD patients. In addition, we showed that functional connectivity between the medial prefrontal and salience networks had the highest power to differentiate PD patients from healthy controls. Our finding may provide useful information for understanding neural system alternations at the modular level in patients with Parkinson's disease.

#### Compliance with ethical standards

**Ethical approval** All procedures performed in studies involving human participants were in accordance with the ethical standards of the institutional or national research committee and with the 1964 Helsinki declaration and its later amendments or comparable ethical standards.

**Funding** This study was funded by the National Natural Science Foundation of China (Grant numbers: 81271548, 81271560, 81371535, 81428013, and 81471654), and Zhejiang Provincial Natural Science Foundation of China (No. LZ13C090001).

**Conflict of interest** All of the authors declare no conflicts of interest.

**Informed consent** Informed consent was obtained from all individual participants included in the study.

## References

- Achard, S., Salvador, R., Whitcher, B., Suckling, J., & Bullmore, E. (2006). A resilient, low-frequency, small-world human brain functional network with highly connected association cortical hubs. *The Journal of Neuroscience*, *26*(1), 63–72.
- Alexander-Bloch, A. F., Gogtay, N., Meunier, D., Birn, R., Clasen, L., Lalonde, F., Lenroot, R., Giedd, J., & Bullmore, E. T. (2010). Disrupted modularity and local connectivity of brain functional networks in childhood-onset schizophrenia. *Frontiers in Systems Neuroscience*, *4*(147), 1–16.
- Ashburner, J. (2007). A fast diffeomorphic image registration algorithm. *NeuroImage*, *38*(1), 95–113.
- Ashburner, J., & Friston, K. J. (2000). Voxel-based morphometry—the methods. *NeuroImage*, *11*(6), 805–821.
- Baggio, H. C., Sala-Llonch, R., Segura, B., Martí, M. J., Valldeoriola, F., Compta, Y., Tolosa, E., & Junqué, C. (2014). Functional brain networks and cognitive deficits in Parkinson's disease. *Human Brain Mapping*, *35*(9), 4620–4634.
- Benjamini, Y., & Hochberg, Y. (1995). Controlling the false discovery rate: a practical and powerful approach to multiple testing. *Journal of the Royal Statistical Society, Series B: Statistical Methodology*, *57*, 289–300.
- Biundo, R., Calabrese, M., Weis, L., Facchini, S., Ricchieri, G., Gallo, P., & Antonini, A. (2013). Anatomical correlates of cognitive functions in early Parkinson's disease patients. *PLoS One*, *8*(8), e64222.
- Boller, F., Passafiume, D., Keefe, N. C., Rogers, K., Morrow, L., & Kim, Y. (1984). Visuospatial impairment in Parkinson's disease: role of perceptual and motor factors. *Archives of Neurology*, *41*(5), 485–490.
- Borghammer, P., Cumming, P., Østergaard, K., Gjedde, A., Rodell, A., Bailey, C. J., & Vafeae, M. S. (2012). Cerebral oxygen metabolism in patients with early Parkinson's disease. *Journal of the Neurological Sciences*, *313*(1), 123–128.
- Braak, H., Tredici, D. K., Rüb, U., de Vos, A. I. R., Steur, N. H. J. E., & Braak, E. (2003). Staging of brain pathology related to sporadic Parkinson's disease. *Neurobiology of Aging*, *24*(2), 197–211.
- Bullmore, E. T., & Bassett, D. S. (2011). Brain graphs: graphical models of the human brain connectome. *Annual Review of Clinical Psychology*, *7*(7), 113–140.
- Bullmore, E., & Sporns, O. (2009). Complex brain networks: graph theoretical analysis of structural and functional systems. *Nature Reviews Neuroscience*, *10*(3), 186–198.
- Cardoso, E. F., Maia, F. M., Fregni, F., Myczkowski, M. L., Melo, L. M., Sato, J. R., Marcolin, M. A., Rigonatti, S. P., Cruz Jr., A. C., & Barbosa, E. R. (2009). Depression in Parkinson's disease: convergence from voxel-based morphometry and functional magnetic resonance imaging in the limbic thalamus. *NeuroImage*, *47*(2), 467–472.
- Chen, Z. J., He, Y., Rosa-Neto, P., Gong, G., & Evans, A. C. (2011b). Age-related alterations in the modular organization of structural cortical network by using cortical thickness from MRI. *NeuroImage*, *56*(1), 235–245.
- Chen, G., Ward, B. D., Xie, C., Li, W., Wu, Z., Jones, J. L., Franczak, M., Antuono, P., & Li, S.-J. (2011a). Classification of Alzheimer disease, mild cognitive impairment, and normal cognitive status with

- large-scale network analysis based on resting-state functional MR imaging. *Radiology*, 259(1), 213–221.
- Chen, Z. J., He, Y., Rosa-Neto, P., Germann, J., & Evans, A. C. (2008). Revealing modular architecture of human brain structural networks by using cortical thickness from MRI. *Cerebral Cortex*, 18(10), 2374–2381.
- Chen, G., Zhang, H.-Y., Xie, C., Chen, G., Zhang, Z.-J., Teng, G.-J., & Li, S.-J. (2013). Modular reorganization of brain resting state networks and its independent validation in Alzheimer's disease patients. *Frontiers in Human Neuroscience*, 7, 456.
- Christopher, L., Marras, C., Duff-Canning, S., Koshimori, Y., Chen, R., Boileau, I., Segura, B., Monchi, O., Lang, A. E., & Rusjan, P. (2014). Combined insular and striatal dopamine dysfunction are associated with executive deficits in Parkinson's disease with mild cognitive impairment. *Brain*, 137(Pt 2), 565–575.
- Cruse, D., Chennu, S., Chatelle, C., Bekinschtein, T. A., Fernandez-Espejo, D., Pickard, J. D., Laureys, S., & Owen, A. M. (2011). Bedside detection of awareness in the vegetative state: a cohort study. *Lancet*, 378(9809), 2088–2094.
- Dai, Z., Yan, C., Li, K., Wang, Z., Wang, J., Cao, M., Lin, Q., Shu, N., Xia, M., & Bi, Y. (2014). Identifying and Mapping Connectivity Patterns of Brain Network Hubs in Alzheimer's Disease. *Cerebral Cortex*, 2014 epub bhu246.
- Damoiseaux, J., Beckmann, C., Arigita, E. S., Barkhof, F., Scheltens, P., Stam, C., Smith, S., & Rombouts, S. (2008). Reduced resting-state brain activity in the "default network" in normal aging. *Cerebral Cortex*, 18(8), 1856–1864.
- Doyon, J., Gaudreau, D., Castonguay, M., Bedard, P., Bédard, F., & Bouchard, J. (1997). Role of the striatum, cerebellum, and frontal lobes in the learning of a visuomotor sequence. *Brain and Cognition*, 34(2), 218–245.
- Dubbelink, K. T. O., Hillebrand, A., Stoffers, D., Deijen, J. B., Twisk, J. W., Stam, C. J., & Berendse, H. W. (2013). Disrupted brain network topology in Parkinson's disease: a longitudinal magnetoencephalography study. *Brain*, 137(1), 197–207.
- Euston, D. R., Gruber, A. J., McNaughton, B. L. (2012). The role of medial prefrontal cortex in memory and decision making. *Neuron*, 76(6), 1057–1070.
- Feamley, J. M., & Lees, A. J. (1991). Ageing and Parkinson's disease: substantia nigra regional selectivity. *Brain*, 114(5), 2283–2301.
- Ferri, F., Frassinetti, F., Ardizzi, M., Costantini, M., & Gallese, V. (2012). A sensorimotor network for the bodily self. *Journal of Cognitive Neuroscience*, 24(7), 1584–1595.
- Foti, N. J., Hughes, J. M., & Rockmore, D. N. (2011). Nonparametric sparsification of complex multiscale networks. *PLoS One*, 6(2), e16431.
- Fox, M. D., Zhang, D., Snyder, A. Z., & Raichle, M. E. (2009). The global signal and observed anticorrelated resting state brain networks. *Journal of Neurophysiology*, 101(6), 3270–3283.
- Friston, K. J., Williams, S., Howard, R., Frackowiak, R. S., & Turner, R. (1996). Movement related effects in fMRI time series. *Magnetic Resonance in Medicine*, 35(3), 346–355.
- Gorges, M., Müller, H. P., Lulé, D., Consortium, L., Pinkhardt, E. H., Ludolph, A. C., & Kassubek, J. (2015). To rise and to fall: functional connectivity in cognitively normal and cognitively impaired patients with Parkinson's disease. *Neurobiology of Aging*, 36(4), 1727–1735.
- Göttlich, M., Münte, T. F., Heldmann, M., Kasten, M., Hagenah, J., & Krämer, U. M. (2013). Altered resting state brain networks in Parkinson's disease. *PLoS One*, 8(10), e77336.
- Guimera, R., & Amaral, L. A. N. (2005). Functional cartography of complex metabolic networks. *Nature*, 433(7028), 895–900.
- de Haan, W., van der Flier, W. M., Koene, T., Smits, L., Scheltens, P., & Stam, C. J. (2012). Disrupted modular brain dynamics reflect cognitive dysfunction in Alzheimer's disease. *NeuroImage*, 59(4), 3085–3093.
- Hawkes, C. H., Tredici, K. D., & Braak, H. (2009). Parkinson's disease. *Annals of the New York Academy of Sciences*, 1170(1), 615–622.
- He, Y., Wang, J., Wang, L., Chen, Z. J., Yan, C., Yang, H., Tang, H., Zhu, C., Gong, Q., & Zang, Y. (2009). Uncovering intrinsic modular organization of spontaneous brain activity in humans. *PLoS One*, 4, e5226.
- Helmich, R. C., Derikx, L. C., Bakker, M., Scheeringa, R., Bloem, B. R., & Toni, I. (2010). Spatial remapping of cortico-striatal connectivity in Parkinson's disease. *Cerebral Cortex*, 20(5), 1175–1186.
- Hoehn, M. M., & Yahr, M. D. (1998). Parkinsonism: onset, progression, and mortality. *Neurology*, 50(2), 318–318.
- Jenkins, A. C., & Mitchell, J. P. (2011). Medial prefrontal cortex subserves diverse forms of self-reflection. *Social Neuroscience*, 6(3), 211–218.
- Jucker, M., & Walker, L. C. (2013). Self-propagation of pathogenic protein aggregates in neurodegenerative diseases. *Nature*, 501(7465), 45–51.
- Kikuchi, A., Takeda, A., Kimpara, T., Nakagawa, M., Kawashima, R., Sugiura, M., Kinomura, S., Fukuda, H., Chida, K., & Okita, N. (2001). Hypoperfusion in the supplementary motor area, dorsolateral prefrontal cortex and insular cortex in Parkinson's disease. *Journal of the Neurological Sciences*, 193(1), 29–36.
- Kurani, A. S., Seidler, R. D., Burciu, R. G., Comella, C. L., Corcos, D. M., Okun, M. S., MacKinnon, C. D., & Vaillancourt, D. E. (2015). Subthalamic nucleus—sensorimotor cortex functional connectivity in de novo and moderate Parkinson's disease. *Neurobiology of Aging*, 36(1), 462–469.
- Lebedev, A. V., Westman, E., Simmons, A., Lebedeva, A., Siepel, F. J., Pereira, J. B., & Aarsland, D. (2014). Large-scale resting state network correlates of cognitive impairment in Parkinson's disease and related dopaminergic deficits. *Frontiers in Systems Neuroscience*, 8, 45.
- Long, D., Wang, J., Xuan, M., Gu, Q., Xu, X., Kong, D., & Zhang, M. (2012). Automatic classification of early Parkinson's disease with multi-modal MR imaging. *PLoS One*, 7, e47714.
- Luo, C. Y., Guo, X. Y., Song, W., Chen, Q., Cao, B., Yang, J., Gong, Q. Y., & Shang, H.-F. (2015). Functional connectome assessed using graph theory in drug-naive Parkinson's disease. *Journal of Neurology*, 262(6), 1557–1567.
- Mesulam, M.-M. (1998). From sensation to cognition. *Brain*, 121(6), 1013–1052.
- Murphy, K., Birn, R. M., Handwerker, D. A., Jones, T. B., & Bandettini, P. A. (2009). The impact of global signal regression on resting state correlations: are anti-correlated networks introduced? *NeuroImage*, 44(3), 893–905.
- Newman, M. E. (2004). Analysis of weighted networks. *Physical Review E, Statistical, Nonlinear, and Soft Matter Physics*, 70(5), 056131.
- Newman, M. E. J. (2006). Finding community structure in networks using the eigenvectors of matrices. *Physical Review E*, 74(3), 036104.
- Polito, C., Berti, V., Ramat, S., Vanzi, E., De Cristofaro, M. T., Pellicano, G., Mungai, F., Marini, P., Formiconi, A. R., & Sorbi, S. (2012). Interaction of caudate dopamine depletion and brain metabolic changes with cognitive dysfunction in early Parkinson's disease. *Neurobiology of Aging*, 33(1), 206. e229–206. e239.
- Pont-Sunyer, C., Hotter, A., Gaig, C., Seppi, K., Compta, Y., Katzenschlager, R., Mas, N., Hofeneder, D., Brücke, T., & Bayés, A. (2014). The onset of nonmotor symptoms in Parkinson's disease (the ONSET PD Study). *Movement Disorders*, 30(2), 229–237.
- Power, J. D., Schlaggar, B. L., & Petersen, S. E. (2015). Recent progress and outstanding issues in motion correction in resting state fMRI. *NeuroImage*, 105, 536–551.
- Putcha, D., Ross, R. S., Cronin-Golomb, A., Janes, A. C., & Stern, C. E. (2015). Altered intrinsic functional coupling between core neurocognitive networks in Parkinson's disease. *NeuroImage Clin*, 7, 449–455.

- Pyatigorskaya, N., Gallea, C., Garcia-Lorenzo, D., Vidailhet, M., & Lehericy, S. (2013). A review of the use of magnetic resonance imaging in Parkinson's disease. *Ther. Adv Neurol Disord*, *2014*, *7*(4), 206–220.
- Radebaugh, T., & Khachaturian, Z. (1998). Consensus report of the Working Group on: molecular and biochemical markers of Alzheimer's disease. *Neurobiology of Aging*, *19*(2), 109–116.
- Rae, C. L., Correia, M. M., Alena, E., Hughes, L. E., Barker, R. A., & Rowe, J. B. (2012). White matter pathology in Parkinson's disease: the effect of imaging protocol differences and relevance to executive function. *NeuroImage*, *62*(3), 1675–1684.
- Raichle, M. E., & Snyder, A. Z. (2007). A default mode of brain function: a brief history of an evolving idea. *NeuroImage*, *37*(4), 1083–1090.
- Rektorova, I., Biundo, R., Marecek, R., Weis, L., Aarsland, D., & Antonini, A. (2014). Grey matter changes in cognitively impaired Parkinson's disease patients. *PLoS One*, *9*(1), e85595.
- Rubinov, M., & Sporns, O. (2010). Complex network measures of brain connectivity: uses and interpretations. *NeuroImage*, *52*(3), 1059–1069.
- Satterthwaite, T. D., Wolf, D. H., Loughhead, J., Ruparel, K., Elliott, M. A., Hakonarson, H., Gur, R. C., & Gur, R. E. (2012). Impact of in-scanner head motion on multiple measures of functional connectivity: relevance for studies of neurodevelopment in youth. *NeuroImage*, *60*(1), 623–632.
- Seeley, W. W., Menon, V., Schatzberg, A. F., Keller, J., Glover, G. H., Kenna, H., Reiss, A. L., & Greicius, M. D. (2007). Dissociable intrinsic connectivity networks for salience processing and executive control. *The Journal of Neuroscience*, *27*(9), 2349–2356.
- Skidmore, F., Korenkevych, D., Liu, Y., He, G., Bullmore, E., & Pardalos, P. M. (2011). Connectivity brain networks based on wavelet correlation analysis in Parkinson fMRI data. *Neuroscience Letters*, *499*(1), 47–51.
- Somerville, L. H., Jones, R. M., Ruberry, E. J., Dyke, J. P., Glover, G., & Casey, B. (2013). The medial prefrontal cortex and the emergence of self-conscious emotion in adolescence. *Psychological Science*, *24*(8), 1554–1562.
- Sporns, O. (2011). The non-random brain: efficiency, economy, and complex dynamics. *Frontiers in Computational Neuroscience*, *5*(5), 1–13.
- Sporns, O., & Zwi, J. D. (2004). The small world of the cerebral cortex. *Neuroinformatics*, *2*(2), 145–162.
- Tessitore, A., Esposito, F., Vitale, C., Santangelo, G., Amboni, M., Russo, A., Corbo, D., Cirillo, G., Barone, P., & Tedeschi, G. (2012). Default-mode network connectivity in cognitively unimpaired patients with Parkinson disease. *Neurology*, *79*(23), 2226–2232.
- Tinaz, S., Lauro, P., Hallett, M., & Horowitz, S. G. (2015). Deficits in task-set maintenance and execution networks in Parkinson's disease. *Brain Structure and Function*, *220*(1), 1–13.
- Vaessen, M., Braakman, H., Heerink, J., Jansen, J., Debeij-van Hall, M., Hofman, P., Aldenkamp, A., & Backes, W. (2013). Abnormal modular organization of functional networks in cognitively impaired children with frontal lobe epilepsy. *Cerebral Cortex*, *23*(8), 1997–2006.
- Van Dijk, K. R., Sabuncu, M. R., & Buckner, R. L. (2012). The influence of head motion on intrinsic functional connectivity MRI. *NeuroImage*, *59*(1), 431–438.
- van Eimeren, T., Monchi, O., Ballanger, B., & Strafella, A. P. (2009). Dysfunction of the default mode network in Parkinson disease: a functional magnetic resonance imaging study. *Archives of Neurology*, *66*(7), 877–883.
- Vincent, J. L., Kahn, I., Snyder, A. Z., Raichle, M. E., & Buckner, R. L. (2008). Evidence for a fronto-parietal control system revealed by intrinsic functional connectivity. *Journal of Neurophysiology*, *100*(6), 3328–3342.
- Wang, J. H., Zuo, X. N., Gohel, S., Milham, M. P., Biswal, B. B., & He, Y. (2011). Graph theoretical analysis of functional brain networks: test-retest evaluation on short- and long-term resting-state functional MRI data. *PLoS One*, *6*(7), e21976.
- Wu, T., & Hallett, M. (2013). The cerebellum in Parkinson's disease. *Brain*, *136*(3), 696–709.
- Wu, T., Long, X., Wang, L., Hallett, M., Zang, Y., Li, K., & Chan, P. (2011b). Functional connectivity of cortical motor areas in the resting state in Parkinson's disease. *Human Brain Mapping*, *32*(9), 1443–1457.
- Wu, K., Taki, Y., Sato, K., Sassa, Y., Inoue, K., Goto, R., Okada, K., Kawashima, R., He, Y., & Evans, A. C. (2011a). The overlapping community structure of structural brain network in young healthy individuals. *PLoS One*, *6*(5), e19608.
- Yan, C.-G., Cheung, B., Kelly, C., Colcombe, S., Craddock, R. C., Martino, A. D., Li, Q., Zuo, X.-N., Castellanos, F. X., & Milham, M. P. (2013). A comprehensive assessment of regional variation in the impact of head micromovements on functional connectomics. *NeuroImage*, *76*(1), 183–201.
- Zalesky, A., Fornito, A., Harding, I. H., Cocchi, L., Yücel, M., Pantelis, C., & Bullmore, E. T. (2010). Whole-brain anatomical networks: does the choice of nodes matter? *NeuroImage*, *50*(3), 970–983.
- Zuo, X.-N., Ehmke, R., Mennes, M., Imperati, D., Castellanos, F. X., Sporns, O., & Milham, M. P. (2012). Network centrality in the human functional connectome. *Cerebral Cortex*, *22*(8), 1862–1875.